Intense circularly polarized attosecond pulse generation from solid targets irradiated with a two-color linearly polarized laser

C. L. Zhong,[1,2] B. Qiao,[1,2,3,*] X. R. Xu,[1,4] Y. X. Zhang,[1,2] X. B. Li,[1,2] Y. Zhang,[1,2] C. T. Zhou,[3] S. P. Zhu,[5,6] and X. T. He[1,2,5]

[1]*Center for Applied Physics and Technology, HEDPS, and SKLNPT, School of Physics, Peking University, Beijing 100871, China*
[2]*Collaborative Innovation Center of IFSA (CICIFSA), Shanghai Jiao Tong University, Shanghai 200240, China*
[3]*Center for Advanced Material Diagnostic Technology, Shenzhen Technology University, Shenzhen 518118, China*
[4]*Department of Physics, National University of Defense Technology, Changsha 410073, China*
[5]*Institute of Applied Physics and Computational Mathematics, Beijing 100094, China*
[6]*Graduate School of China Academy of Engineering Physics, P.O. Box 2101, Beijing 100088, China*

(Received 31 July 2019; revised manuscript received 3 August 2019; accepted 23 March 2020; published 5 May 2020)

A method for the production of intense circularly polarized (CP) attosecond pulses from relativistic laser-solid interactions is proposed, where a two-color linearly polarized (LP) laser is used. The polarization, photon frequency, and other properties of the obtained attosecond pulse can be controlled by adjusting the ratio of the dichromatic driving LP field in different harmonics, which is much easier and more efficient than those previously using CP driving lasers. Both one- and two-dimensional particle-in-cell simulations show that a CP attosecond extreme-ultraviolet pulse with an intensity of $1.4 \times 10^{19}\,\mathrm{W/cm^2}$ and a duration of about 120 as is obtained by a two-color LP laser at intensities in the fundamental and second harmonics of, respectively, 1.5×10^{22} and $6.4 \times 10^{21}\,\mathrm{W/cm^2}$, which can be applied for the detection of the magnetic and chiral properties of materials.

DOI: 10.1103/PhysRevA.101.053814

I. INTRODUCTION

Chirality, the asymmetric property by which an object or structure and its mirror image are not superimposable, plays an important role in material science. Circularly polarized (CP) radiation is an extremely powerful tool to investigate the chirality of materials by light-matter interactions, from photoionization in chiral molecules to magnetic properties in solid-state materials [1–5]. In particular, due to high spatial and temporal resolutions, CP radiation in the extreme ultraviolet (XUV) or x-ray spectral range can be used as magnetic circular dichroism spectroscopy [6,7] for detecting absorption edges of atoms, measuring quantum phase in topological insulators, distinguishing ultrafast dynamics of spin and orbital moments, and tracking transient ferromagnetic processes of magnetic systems [8–12]. A CP XUV or x-ray pulse can be obtained on large free-electron laser facilities through adjusting the configuration of undulators and using the metal mirror polarizer [13,14], which, however, generally has a duration in femtosecond scale and is very costly.

High harmonic generation (HHG) from noble gases interacting with linearly polarized (LP) lasers has been explored to obtain XUV pulses, which is based on ionization, acceleration, and recombination of electrons from atoms in laser fields, i.e., the three-step model [15]. In this scheme, the efficiency of HHG decreases exponentially when the laser ellipticity increases; therefore, it meets intrinsic difficulties in generating a CP XUV pulse. Generation of quasi-CP HHG have been proposed by using aligned molecules interacting with rotating dichromatic CP or LP lasers with orthogonal polarizations [16,17]. However, the photon energy and total flux of the obtained CP HHG are rather low due to the limitation of the ionization threshold and conversion efficiency [18,19].

In principle, intense laser-plasma interactions provide a more promising way to achieve XUV pulse radiations with high brightness via the relativistically oscillating mirror (ROM) [20–24] mechanism, because there is no limitation on the applicable drive laser intensity and thus the XUV intensity. To obtain CP HHG, relativistic CP or elliptically polarized (EP) lasers [25,26] are used to obliquely irradiate a plasma surface, where the polarization of HHG is inherited from the driving laser. However, on the one hand, an intense CP or EP drive laser itself is extremely challenging to be available in experiments, where a significant amount of energy is lost when transforming lasers from LP to CP; on the other hand, it is actually very hard to control the generation of CP HHG with both the stable phase difference $\pi/2$ and the equivalent radiation amplitudes in two orthogonal directions at the cycle near the drive laser peak intensity by adjusting solely the incidence angle, resulting in low conversion efficiency and low brilliance of the generated CP HHG.

In this paper, we propose a scheme for generation of relativistically intense CP attosecond XUV pulses by using a LP laser, which can be realized with current laser facilities [27]. In this scheme, an *S*-polarized two-color laser is used to obliquely irradiate a solid target [see Fig. 1(a)], where the laser electric field and the transverse component of the oscillating ponderomotive force drive transverse currents in two orthogonal directions with different harmonics and a

*bqiao@pku.edu.cn

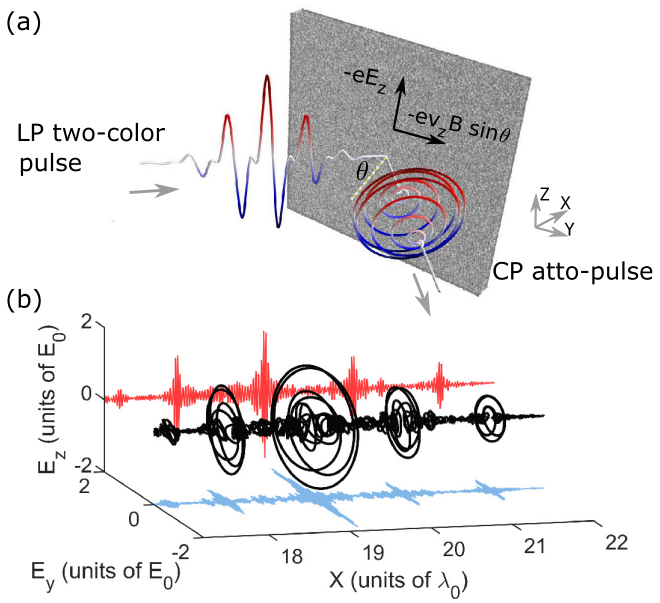

FIG. 1. (a) Schematic for the principle of the proposed scheme: generation of CP attosecond pulse from solid targets by an intense two-color LP laser via ROM. (b) Waveform of the obtained CP attosecond XUV pulse after spectral filtering in 1D PIC simulation, where the 30th–46th harmonic orders are selected. The waveform of the 3D electric field vector (black) and the two orthogonal electric field components E_y (blue, light gray) and E_z (red, dark gray) are displayed. The laser and target parameters in the simulation are described in the text.

phase difference of $\pi/2$, while the longitudinal ponderomotive force drives the oscillating plasma mirror. According to the selection rules [21] of HHG in ROM, both odd and even harmonics are generated in two orthogonal directions. By controlling the ratio of the dichromatic driving field in different harmonics of two-color lasers as well as its incident angle, similar harmonic spectra in two directions can be achieved, resulting in the production of intense CP attosecond pulses. The principle and the condition of the scheme are theoretically given and verified by one-dimensional (1D) and 2D particle-in-cell (PIC) simulations for a large range of laser and target parameters. It is shown that an intense CP attosecond XUV pulse with an intensity of $1.4 \times 10^{19}\,\mathrm{W/cm^2}$ and a duration of about 120 as can be generated by using a two-color S-polarized laser at intensities in the fundamental and second harmonics of, respectively, $I_\omega = 1.5 \times 10^{22}$ and $I_{2\omega} = 6.4 \times 10^{21}\,\mathrm{W/cm^2}$ [see Fig. 1(b)].

II. THEORETICAL ANALYSIS

Let us start by analyzing the harmonic generation dynamics in the boosted frame introduced by Bourdier [28], which well describe the interaction of a solid target with the obliquely incident laser. In the boosted frame, as shown in Fig. 1(a), the target plasma have a drift velocity $-c\sin\theta$ along the Y direction, where θ is the incident angle in the laboratory frame and c is the speed of light. The S-polarized laser propagates along the X direction with electric field along the Z direction. In this case, the electric field wave propagation equation can be written as $(\partial_x^2 - 1/c^2\partial_t^2)\mathbf{A}(x,t) = -(1/\varepsilon_0 c^2)\mathbf{J}_\perp(x,t)$, where $\mathbf{A}$ is the vector potential of the laser field as $\mathbf{E} = -\partial\mathbf{A}/\partial t$, and $\mathbf{J}_\perp$ is the transverse current density. Hereafter, dimensionless quantities are used as $n_e = n_e/n_c$, $\beta = v/c$, $\omega = \omega/\omega_0$, $J = J/(n_{e0}ec)$, $E = E/E_0$, $E_0 = m_e\omega_0 c/e$, $B = B/B_0$, $B_0 = m_e\omega_0/e$, and $\mathbf{a} = e\mathbf{A}/mc$, where $n_c = \omega_0^2\varepsilon_0 m_e/e^2$ is the critical density. Then, the reflected electric field $\mathbf{E}_\perp^{\mathbf{r}}$ can be obtained as

$$\mathbf{E}_\perp^{\mathbf{r}}(x,t) = -\frac{1}{2}\int_{-\infty}^{+\infty} dx'dt' \frac{\partial \mathbf{J}_\perp(x,t,x',t')}{\partial t'}, \tag{1}$$

where $\mathbf{J}_\perp = -en_e\beta_e\delta(x-x') + Zen_i\beta_i$, indexes i and e mean ion and electron, respectively, Z is the atomic number, and $\delta(x-x')$ represents density distribution of the compressed oscillating plasma surface. From Eq. (1), we see that harmonic radiation depends critically on the time derivative of the transverse current density $\partial\mathbf{J}_\perp/\partial t = -en\partial(\mathbf{p}_\perp/\gamma)/\partial t$, where $\mathbf{p}_\perp$ is the electron transverse momentum. In the boosted frame, the plasma has a drift velocity of $\beta_{y0} = -\sin\theta$. Since no electric field exists in the Y direction, we obtain that $p_y = p_{y0} = \gamma_0\beta_{y0} = \sin\theta/\cos\theta = \tan\theta$. Substituting these into Eq (1), we get

$$E_z^r(x,t) = \frac{1}{2}\int_{-\infty}^{+\infty} dx' \frac{n_e p_z}{(1+\beta_x)\gamma}\delta(x-x'), \tag{2}$$

$$E_y^r(x,t) = \frac{1}{2}\int_{-\infty}^{+\infty} dx' \frac{n_e \tan\theta}{(1+\beta_x)\gamma}\delta(x-x'). \tag{3}$$

Since harmonic radiation occurs when the transverse current density has the maximum time derivative, i.e., passing though the zero node, and the radiation process lasts only on an attosecond time scale, the transverse momentum in the Z direction during radiation can be approximated in the first-order expansion as $p_z = dp_z/dt|_{t=t_{\mathrm{rad}}}\Delta t = \omega_d\Delta t$, where $\omega_d = dp_z/dt|_{t=t_{\mathrm{rad}}}$ is defined. Then, after some derivations, we obtain the reflected high harmonic spectra after Fourier transformation as

$$\begin{aligned} E_z^r(\omega) &= \frac{\hat{E}_z^r}{2\pi}\int_{-\infty}^{+\infty} dt'' e^{it''\frac{\omega}{\omega_d\cos(\theta)}}\frac{A_m}{\omega_d}\frac{t''}{1+t''^2} \\ &= \hat{E}_z^r\frac{A_m}{2\omega_d}e^{-\frac{\omega}{\omega_d\cos(\theta)}}e^{i\frac{\pi}{2}}, \end{aligned} \tag{4}$$

$$\begin{aligned} E_y^r(\omega) &= \frac{\hat{E}_y^r}{2\pi}\int_{-\infty}^{+\infty} dt'' e^{it''\frac{\omega}{\omega_d\cos(\theta)}}\frac{A_m}{\omega_d}\frac{\sin(\theta)}{1+t''^2} \\ &= \hat{E}_y^r\frac{A_m}{2\omega_d}e^{-\frac{\omega}{\omega_d\cos(\theta)}}\sin(\theta), \end{aligned} \tag{5}$$

where $\gamma \approx \mathrm{a}$, $t'' = p_z\cos\theta = \omega_d t\cos\theta$, and $A_m = \gamma n_e(1-\beta_x)/2$ is a slowly varying function of time for $\omega \gg \omega_0$ and $a \gg 1$. $\hat{E}_z^r = \mathrm{sign}(dp_z/dt)$ and $\hat{E}_y^r = \mathrm{sign}(dp_y/dt)$ represent the directions of two orthogonal reflected electric fields that can be plus or minus.

The properties of the harmonic radiation in the reflected direction can be analyzed from Eqs. (4) and (5). First, comparing the phase terms in both equations, we see that the phases of the harmonic radiations in the Z and Y directions have a difference of $\Delta\phi_{\mathrm{rad}} = \pi/2$ or $-\pi/2$. When transforming back to the laboratory frame with $E_y' = E_y\cos\theta$ and $E_z' = \gamma_0 E_z + \beta_0 cB_x = E_z\cos\theta$, where $B_x = 0$ in the boosted frame,

this $\pi/2$ or $-\pi/2$ phase difference for the radiations in two directions is still kept, which is consistent with the phase of the driving S-polarized laser [29]. Note that the origin of $\Delta\phi_{\rm rad}$ can be directly explained from the acting force on the oscillating plasma surface in the laboratory frame, where the laser electric field $f_z = -eE_z$ and the transverse ponderomotive force $f_y = -ev_z B\sin\theta$ drive transverse currents in two orthogonal directions with different harmonics and a stable $\Delta\phi_{\rm rad}$ of $\pi/2$, while the longitudinal ponderomotive force drives the oscillating plasma mirror.

Second, to obtain CP harmonic radiation, the radiation fields in two orthogonal directions also need to have the same amplitudes at the same harmonic orders. If using one-color lasers, t'' in Eqs. (4) and (5) can be written as $\cos(\omega t)$, and correspondingly the terms in the integrand become $1/(1+t''^2) = \Sigma(-1)^n\cos(\omega t)^{2n}$ and $t''/(1+t''^2) = \Sigma(-1)^n\cos(\omega t)^{2n+1}$. Then, we conclude that there always exists a harmonic mismatch between the radiations in the Z direction (ω, 3ω, 5ω, …) and the Y direction (2ω, 4ω, 6ω, …), obeying the harmonic selection rules [21]. Moreover, the ratio of the radiation field amplitudes is always $E_y/E_z = \sin\theta$. Therefore, to achieve the same radiation amplitudes in both Y and Z directions as well as at the same harmonic orders, we propose using a two-color laser with the field amplitude $a = a_1\cos(\omega_1 t) + a_2\cos(\omega_2 t + \phi_0)$, where the initial phase ϕ_0 is used to control the radiation cycle by changing the wave form of the incident two-color laser field, and the intensity ratio of two-color laser field $W = I_{\omega 2}/(I_{\omega 1} + I_{\omega 2}) = a_2^2/(a_1^2 + a_2^2)$ can be adjusted to achieve the same radiation amplitude in two directions. Furthermore, the efficiency of HHG can also be enhanced by the two-color laser setup itself [30–33]. Therefore, an intense CP attosecond pulse can be obtained by our proposed scheme, as shown in Fig. 1(b).

III. SIMULATION RESULTS

To verify the above theory of our scheme, 1D PIC simulations are carried out by using the code EPOCH [34]. The simulation box has a length of 60λ ($0 \leqslant x \leqslant 60\lambda$), which is composed of 240 000 cells. Each cell of the plasma is filled with 200 quasiparticles for both electrons and ions. An S-polarized two-color laser with peak intensities of, respectively, $I_{\omega_1} = I_\omega = 1.5\times10^{22}$ and $I_{\omega_2} = I_{2\omega} = 6.4\times10^{21}\,{\rm W/cm^2}$ ($W = 0.3$) propagates from the left boundary at $x = 0$ and obliquely irradiates a solid target at $x = 50\lambda$ with an incident angle of $\theta = 45^\circ$, where $\lambda = 800$ nm is the wavelength of the fundamental component. The laser pulse has a temporally Gaussian profile as $I(t) = I_0\exp[-4ln2(t/\tau_p)^2]$ in both the fundamental ($I_0 = I_\omega$) and the second harmonic ($I_0 = I_{2\omega}$) components, where $\tau_p = 18$ fs is chosen here. The electron density of the solid target is assumed to be $n_{e0} = 195n_c$ with a preplasma of $n_e = n_{e0}e^{-(x-50\lambda)/l_s}$ and $l_s = 0.1\lambda$. Simulations for the one-color laser case are also carried out for comparison, where the peak intensity is chosen as $I = I_\omega + I_{2\omega} = 2.14\times10^{22}\,{\rm W/cm^2}$ so that the total laser energy stays the same. Note that for the laser pulse with a Gaussian temporal profile, according to the basic principle of the Fourier analysis [35], the bandwidth of the laser frequency is self-consistently included. For $\tau_p = 18$ fs, we can easily obtain that the laser bandwidth for the fundamental and second harmonic components are respectively $\Delta\lambda_{800} = 52.3$ nm and $\Delta\lambda_{400} = 13.1$ nm.

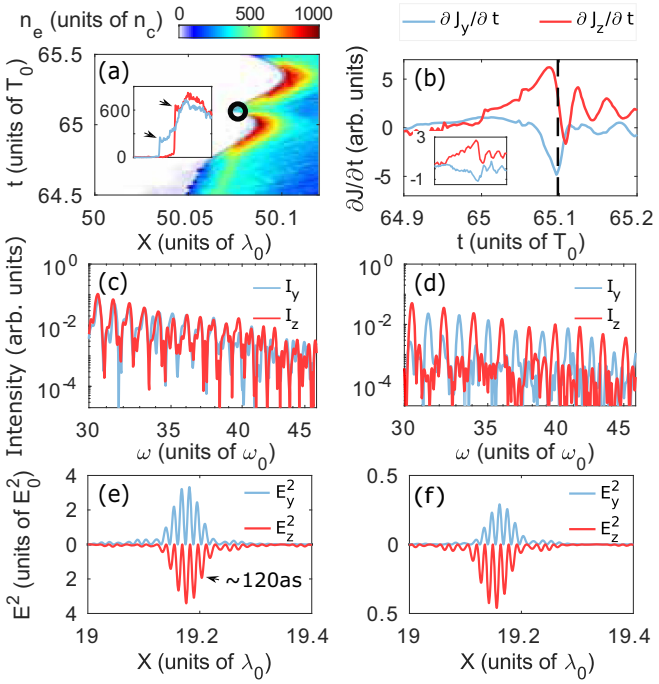

FIG. 2. 1D PIC simulation results for the proposed scheme, where the simulation parameters are shown in the text. (a) Spatiotemporal distribution of the electron density n_e and (b) time derivations of the current density $\partial J/\partial t$. The inset of panel (a) shows the electron density n_e along the surface in one-color (blue, light gray) and two-color (red, dark gray) laser cases, respectively, where arrows indicate the location of the mirror surface. The inset of panel (b) shows $\partial J/\partial t$ of the one-color case. (c) and (d) The obtained harmonic spectra in the specular direction at $t = 96T_0$ for the two- and one-color laser cases, respectively. (e) and (f) The normalized field intensities $|E_y|^2$ (upper panel) and $|E_z|^2$ (lower panel) of the attosecond pulse after selecting 30th–46th harmonic orders emitted around the peak laser intensity for the two- and one-color laser cases, respectively.

Figure 2(a) plots electron density distributions evolving with time t from $t = 64.5T_0$ to $65.5T_0$ at the cycle of the peak laser intensity. We see clearly that an oscillating plasma mirror at target surface forms and high harmonic radiation occurs at $t \approx 65.1T_0$ (see the black circle). The time derivatives of the transverse current densities evolving with time in the Y and Z directions are plotted in Fig. 2(b), which shows that they have a phase difference of $\pi/2$, consistent with the above theoretical expectation [Eqs. (4) and (5)]. Furthermore, it can be seen from Fig. 2(c) that the obtained harmonic spectra in the Y and Z directions have almost the same magnitude at both odd and even harmonics, while those in the one-color laser case always mismatch with each other [see Fig. 2(d)]. On the other hand, comparing Figs. 2(c) and 2(d), we also see the harmonic radiation is significantly enhanced by using two-color lasers due to the higher compressed electron density of the plasma mirror [see inset of Fig. 2(a)] and the larger transverse current density gradients [inset of Fig. 2(b)]. Eventually, as shown in Figs. 2(e) and 1(b), an intense CP attosecond pulse with an intensity of $I \approx 1.4\times10^{19}\,{\rm W/cm^2}$ and a duration of full

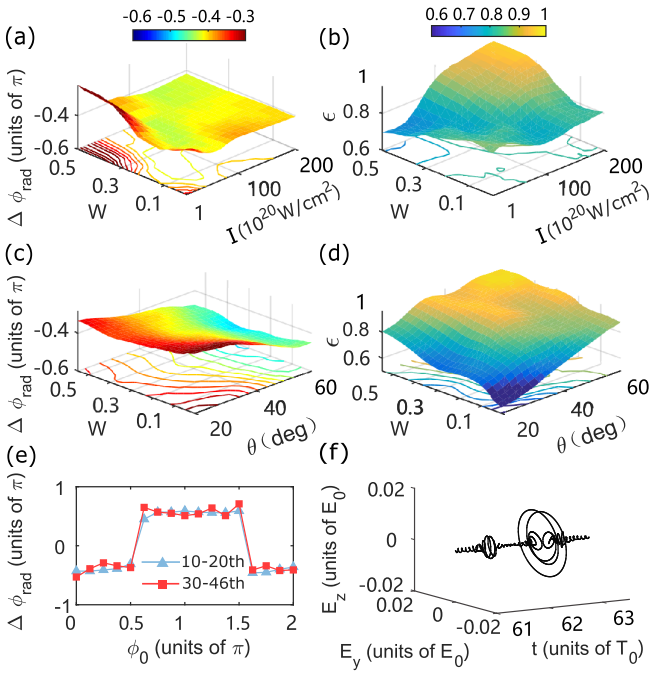

FIG. 3. One-dimensional PIC simulation results for a wide range of laser parameters including intensities I, incident angles θ, and intensity ratios of the two-color field W. Panels (a) and (b) show dependencies of, respectively, the phase difference $\Delta\phi_{\rm rad}$ and the ellipticity ϵ of the obtained attosecond pulse after spectral filtering on laser intensities I as well as intensity ratios W. Panels (c) and (d) show those dependencies on the incident angles θ as well as W. (e) $\Delta\phi_{\rm rad}$ in two orthogonal directions with harmonics 10th–20th (blue triangles, light gray) and 30th–46th (red squares, dark gray) depending on the initial phase ϕ_0 of the two-color laser, where $I = 2.14 \times 10^{22}$ W/cm^2 and $W = 0.3$ are taken. (f) Wave form of the obtained CP attosecond XUV pulse after spectral filtering with 15th–20th harmonics, where lower intensities of $I = 8.55 \times 10^{18}$ W/cm^2 and $W = 0.3$ are taken.

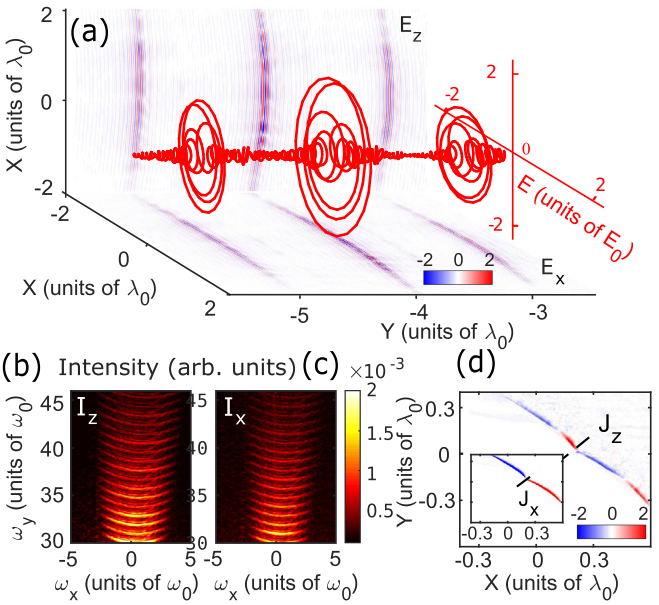

FIG. 4. Two-dimensional PIC simulation results. (a) Spatial distribution of the electric fields E_z and E_x of the obtained attosecond pulses after spectral filtering (selecting 30th–46th harmonic orders) and wave form of the 3D electric field vector (red) along the Y axis. (b) and (c) The corresponding high harmonic spectra in two directions. (d) Current densities of the oscillating plasma surface.

width at half maximum ≈120 as are obtained after selecting the harmonic orders from 30th to 46th with the spectral filtering, where the phase difference $\Delta\phi_{\rm rad}$ between E_y and E_z is -0.42π and the ellipticity $\epsilon \equiv |\min(E_y, E_z)/\max(E_y, E_z)|$ is 1.

To check the robustness, a series of 1D PIC simulations are carried out for a large range of laser intensities I and incident angles θ. From Figs. 3(a) and 3(b), we see that for laser amplitudes varying from 1×10^{20} to 2.14×10^{22} W/cm^2, through adjusting the intensity ratio of the dichromatic driving laser fields from $W = 0.3$ to 0.5, CP attosecond pulses with phase differences within -0.4π to -0.5π and ellipticities ϵ larger than 0.9 are always obtained. Also from Figs. 3(c) and 3(d), we conclude that in the range of incidence angle of 45°-60° and intensity ratio W of 0.2–0.5, the phase difference is stable within -0.45π to -0.5π and the ellipticity ϵ is stable within 0.9 to 1. Figure 3(e) plots the phase difference of the obtained CP attosecond pulses in two directions varying with various initial phases ϕ_0 of the laser in the 2ω component, where two harmonic order ranges of 10th–20th and 30th–46th are selected. We see that a relatively stable phase difference of about $\pi/2$ or $-\pi/2$ can be obtained, within our expectation.

Meanwhile it also indicates that the chirality of the attosecond pulse can be rotated by the initial phase. This can be attributed to the change of the radiation dynamics for two-color lasers in which harmonic radiation is generated in half a laser cycle. To show that our scheme also works at lower intensities, the simulation at the drive laser intensity of $I = 8.55 \times 10^{18}$ W/cm^2 is also carried out, and the results are shown in Fig. 3(f). The obtained attosecond pulse has a duration of about 200 as, a phase difference of 0.55π, and an ellipticity of 0.95. Note that, considering the condition for the driving forces in both orthogonal directions to be comparable as well as the condition for ROM occurrence, the intensity of the incident laser should exceed the relativistic limit. Experimentally, mixing and controllability of relativistic two-color fields can be achieved in terawatt (TW) and petawatt (PW) laser systems. For the weakly relativistic TW laser system, there are no severe coaxial difficulties for the combination of two components as in the experimental setup shown in Ref. [31]. However, for the highly relativistic PW laser system, the second harmonic component should be generated before the compressing like the setup in Ref. [36]. Furthermore, the time delay should be compensated and the B-integral issue needs to be avoided.

To further take the multidimensional effects into account, 2D PIC simulations are also carried out, where a two-color S-polarized laser with transversely Gaussian spatial distribution of radius $r = 3\lambda$ is used. It is worth noting that 2D simulations for HHG are computationally expensive and the resolution is limited. To save the computational resources, five times lower resolutions in space (800 cells/λ) and time than 1D are used. The simulation box size is $12\lambda \times 25\lambda$ along the X and Y axes,

composed of $9600 \times 20\,000$ cells. Each plasma cell is filled with only 32 quasiparticles. Other parameters are the same as those in the above 1D simulations. The simulation results are shown in Fig. 4. It can be clearly seen that an intense CP attosecond XUV pulse [red curves in Fig. 4(a)] at an intensity of $1.2 \times 10^{19}\,\mathrm{W/cm^2}$ [4(a)], a duration of about 150 as, and a photon frequency within $30\omega \sim 46\omega$ [Figs. 4(b) and 4(c)] is also generated in two dimensions. Figures 4(b)–4(d) prove that the radiation spectra and the transverse current densities match well in two directions with a phase difference of $\pi/2$, resulting in the production of CP attosecond XUV pulses.

IV. CONCLUSION

In summary, a method for the production of intense CP attosecond XUV pulses from solid targets irradiated with a relativistic two-color LP laser has been reported. The polarization, photon frequency, and brilliance of the generated CP attosecond pulse can be controlled by adjusting the ratio of the dichromatic driving LP field in different harmonics, the incidence angle, and the initial phase, which is inherently different from previously using a CP driving laser. Such an intense CP attosecond XUV pulse has a great application prospect to characterize the chiral, magnetic properties of materials.

ACKNOWLEDGMENTS

This work is supported by Science Challenge Project, No. TZ2018005; NSAF, Grant No. U1630246; National Natural Science Foundation of China, Grant No. 11921006; the Strategic Priority Research Program of Chinese Academy of Sciences Grant No. XDA25050900; the National Key R&D Program of China, Grant No. 2016YFA0401100; BQ acknowledges Supported from National Natural Science Funds for Distinguished Young Scholar, Grant No. 11825502. The simulations are carried out on the Tianhe-2 supercomputer at the National Supercomputer Center in Guangzhou.

[1] R. Kienberger, E. Goulielmakis, M. Uiberacker, A. Baltuska, V. Yakovlev, F. Bammer, A. Scrinzi, T. Westerwalbesloh, U. Kleineberg, U. Heinzmann *et al.*, Nature (London) **427**, 817 (2004).
[2] M. Cho, Nat. Phys. **11**, 621 (2015).
[3] R. Cireasa, A. E. Boguslavskiy, B. Pons, M. C. H. Wong, D. Descamps, S. Petit, H. Ruf, N. Thiré, A. Ferré, J. Suarez *et al.*, Nat. Phys. **11**, 654 (2015).
[4] I. Gierz, M. Lindroos, H. Höchst, C. R. Ast, and K. Kern, Nano Lett. **12**, 3900 (2012).
[5] N. Böwering, T. Lischke, B. Schmidtke, N. Müller, T. Khalil, and U. Heinzmann, Phys. Rev. Lett. **86**, 1187 (2001).
[6] G. Schütz, M. Knülle, and H. Ebert, Phys. Scr. **1993**, 302 (1993).
[7] P. Stephens, Annu. Rev. Phys. Chem. **25**, 201 (1974).
[8] C. T. Chen, F. Sette, Y. Ma, and S. Modesti, Phys. Rev. B **42**, 7262 (1990).
[9] S.-Y. Xu, M. Neupane, C. Liu, D. Zhang, A. Richardella, L. A. Wray, N. Alidoust, M. Leandersson, T. Balasubramanian, J. Sánchez-Barriga *et al.*, Nat. Phys. **8**, 616 (2012).
[10] C. Boeglin, E. Beaurepaire, V. Halté, V. López-Flores, C. Stamm, N. Pontius, H. Dürr, and J.-Y. Bigot, Nature (London) **465**, 458 (2010).
[11] I. Radu, K. Vahaplar, C. Stamm, T. Kachel, N. Pontius, H. A. Dürr, T. A. Ostler, J. Barker, R. F. L. Evans, R. W. Chantrell *et al.*, Nature (London) **472**, 205 (2011).
[12] B. Pfau, S. Schaffert, L. Müller, C. Gutt, A. Al-Shemmary, F. Büttner, R. Delaunay, S. Düsterer, S. Flewett, R. Frömter *et al.*, Nat. Commun. **3**, 1100 (2012).
[13] C. von Korff Schmising, D. Weder, T. Noll, B. Pfau, M. Hennecke, C. Strüber, I. Radu, M. Schneider, S. Staeck, C. M. Günther *et al.*, Rev. Sci. Instrum. **88**, 053903 (2017).
[14] E. Allaria, B. Diviacco, C. Callegari, P. Finetti, B. Mahieu, J. Viefhaus, M. Zangrando, G. De Ninno, G. Lambert, E. Ferrari *et al.*, Phys. Rev. X **4**, 041040 (2014).
[15] P. B. Corkum, Phys. Rev. Lett. **71**, 1994 (1993).
[16] X. Zhang, X. Zhu, X. Liu, D. Wang, Q. Zhang, P. Lan, and P. Lu, Opt. Lett. **42**, 1027 (2017).
[17] G. Lambert, B. Vodungbo, J. Gautier, B. Mahieu, V. Malka, S. Sebban, P. Zeitoun, J. Luning, J. Perron, A. Andreev *et al.*, Nat. Commun. **6**, 6167 (2015).
[18] P. Tzallas, E. Skantzakis, L. Nikolopoulos, G. D. Tsakiris, and D. Charalambidis, Nat. Phys. **7**, 781 (2011).
[19] D. Fabris, T. Witting, W. Okell, D. Walke, P. Matia-Hernando, J. Henkel, T. Barillot, M. Lein, J. Marangos, and J. Tisch, Nat. Photonics **9**, 383 (2015).
[20] S. V. Bulanov, N. M. Naumova, and F. Pegoraro, Phys. Plasmas **1**, 745 (1994).
[21] R. Lichters, J. Meyer-ter Vehn, and A. Pukhov, Phys. Plasmas **3**, 3425 (1996).
[22] T. Baeva, S. Gordienko, and A. Pukhov, Phys. Rev. E **74**, 046404 (2006).
[23] B. Dromey, M. Zepf, A. Gopal, K. Lancaster, M. Wei, K. Krushelnick, M. Tatarakis, N. Vakakis, S. Moustaizis, R. Kodama *et al.*, Nat. Phys. **2**, 456 (2006).
[24] B. Dromey, S. Kar, C. Bellei, D. C. Carroll, R. J. Clarke, J. S. Green, S. Kneip, K. Markey, S. R. Nagel, P. T. Simpson *et al.*, Phys. Rev. Lett. **99**, 085001 (2007).
[25] Z.-Y. Chen and A. Pukhov, Nat. Commun. **7**, 12515 (2016).
[26] G. Ma, W. Yu, M. Yu, B. Shen, and L. Veisz, Opt. Express **24**, 10057 (2016).
[27] V. Yanovsky, V. Chvykov, G. Kalinchenko, P. Rousseau, T. Planchon, T. Matsuoka, A. Maksimchuk, J. Nees, G. Cheriaux, G. Mourou *et al.*, Opt. Express **16**, 2109 (2008).
[28] A. Bourdier, Phys. Fluids **26**, 1804 (1983).
[29] S. Tang and N. Kumar, Plasma Phys. Control. Fusion **61**, 025013 (2019).
[30] M. R. Edwards, V. T. Platonenko, and J. M. Mikhailova, Opt. Lett. **39**, 6823 (2014).

[31] M. Yeung, S. Rykovanov, J. Bierbach, L. Li, E. Eckner, S. Kuschel, A. Woldegeorgis, C. Rödel, A. Sävert, G. G. Paulus *et al.*, Nat. Photonics **11**, 32 (2017).

[32] E. Agrawal, N. Verma, and P. Jha, Laser Part. Beams **35**, 182 (2017).

[33] S. Mirzanejad and M. Salehi, Phys. Rev. A **87**, 063815 (2013).

[34] T. D. Arber, K. Bennett, C. S. Brady, A. Lawrence-Douglas, M. G. Ramsay, N. J. Sircombe, P. Gillies, R. G. Evans, H. Schmitz, A. R. Bell *et al.*, Plasma Phys. Control. Fusion **57**, 113001 (2015).

[35] Z. Chang, *Fundamentals of Attosecond Optics* (CRC, Boca Raton, FL, 2016).

[36] S. Li, G. Li, Q. Ain, M. S. Hur, A. C. Ting, V. V. Kulagin, C. Kamperidis, and N. A. M. Hafz, Sci. Adv. **5**, eaav7940 (2019).